ISSN 1674-1056
http://cpb.iphy.ac.cn
http://iopscience.iop.org/cpb
中国物理 B
Chinese Physics
中国物理
Chinese Physics B

The n-type Si-based materials applied on the front surface of IBC-SHJ solar cells

Jianhui Bao(包建辉), Ke Tao(陶科), Yiren Lin(林苡任), Rui Jia(贾锐), Aimin Liu(刘爱民)
Citation: Chin. Phys. B . 2019, 28(9): 098201 . **doi:** 10.1088/1674-1056/28/9/098201
Journal homepage: http://cpb.iphy.ac.cn; http://iopscience.iop.org/cpb

What follows is a list of articles you may be interested in

Molecular dynamics simulations on the dynamics of two-dimensional rounded squares

Zhang-lin Hou(侯章林), Ying Ju(句颖), Yi-wu Zong(宗奕吾), Fang-fu Ye(叶方富), Kun Zhao(赵坤)
Chin. Phys. B . 2018, 27(8): 088203 . **doi:** 10.1088/1674-1056/27/8/088203

To what extent of ion neutralization can multivalent ion distributions around RNA-like macroions be described by Poisson-Boltzmann theory?

Gui Xiong(熊贵), Kun Xi(席昆), Xi Zhang(张曦), Zhi-Jie Tan(谭志杰)
Chin. Phys. B . 2018, 27(1): 018203 . **doi:** 10.1088/1674-1056/27/1/018203

Effect of elastic strain energy on grain growth and texture in AZ31 magnesium alloy by phase-field simulation

Ri He(何日), Ming-Tao Wang(王明涛), Jian-Feng Jin(金剑锋), Ya-Ping Zong(宗亚平)
Chin. Phys. B . 2017, 26(12): 128201 . **doi:** 10.1088/1674-1056/26/12/128201

Diffusion in the aged aluminium film on iron

A Y Galashev, O R Rakhmanova, V A Kovrov, Yu P Zaikov
Chin. Phys. B . 2017, 26(3): 038201 . **doi:** 10.1088/1674-1056/26/3/038201

Aggregation of fullerene (C_{60}) nanoparticle：A molecular-dynamic study

He Su-Zhen, Merlitz Holger, Wu Chen-Xu
Chin. Phys. B . 2014, 23(4): 048201 . **doi:** 10.1088/1674-1056/23/4/048201

The n-type Si-based materials applied on the front surface of IBC-SHJ solar cells*

Jianhui Bao(包建辉)[1,2], Ke Tao(陶科)[2,†], Yiren Lin(林苡任)[1], Rui Jia(贾锐)[2,‡], and Aimin Liu(刘爱民)[3,§]

[1] School of Microelectronics, Dalian University of Technology, Dalian 116024, China
[2] Institute of Microelectronics of Chinese Academy of Sciences, Beijing 100029 China
[3] School of Physics & Optoelectronic Engineering, Dalian University of Technology, Dalian 116024, China

(Received 15 May 2019; revised manuscript received 24 June 2019; published online 7 August 2019)

Interdigitated back contact silicon hetero-junction (IBC-SHJ) solar cells exhibit excellent performance owing to the IBC and SHJ structures. The front surface field (FSF) layer composed of electric field passivation and chemical passivation has been proved to play an important role in IBC-SHJ solar cells. The electric field passivated layer n^+-a-Si: H, an n-type Si alloy with carbon or oxygen in amorphous phase, is simulated in this study to investigate its effect on IBC-SHJ. It is indicated that the n^+-a-Si: H layer with wider band gap can reduce the light absorption on the front side efficaciously, which hinders the surface recombination of photo-generated carriers and thus contributes to the improvement of the short circuit current density J_{sc}. The highly doped n^+-a-Si: H can result in the remakable energy band bending, which makes it outstanding in the field passivation, while it makes little contribution to the chemical passivation. It is noteworthy that when the electric field intensity exceeds 1.3×10^5 V/cm, the efficiency decrease caused by the inferior chemical passivation is only 0.16%. In this study, the IBC-SHJ solar cell with a front n^+-a-Si: H field passivation layer is simulated, which shows the high efficiency of 26% in spite of the inferior chemical passivation on the front surface.

Keywords: Si-based doped materials, passivation, interdigitated back contact silicon hetero-junction (IBC-SHJ) solar cell, simulation

PACS: 82.20.Wt, 77.55.df, 82.45.Bb **DOI:** 10.1088/1674-1056/ab33ec

1. Introduction

The interdigitated back contact (IBC) solar cell was first proposed by Lammert and Schwartz in 1975.[1] With the emitter placed at the back, the interdigitated structure is formed, which eliminates the electrode shading and thus can improve the short circuit current density J_{sc}. Sun Power demonstrated that the efficiency of IBC solar cells reached 25.2% in 2016.[2] Silicon hetero-junction (SHJ) solar cells were pioneered in the early 1990s by Sanyo. Panasonic and Kaneka further increased the conversion efficiency up to 24.7% and 25.1%, respectively.[3,4] The SHJ structure, with a hydrogenated amorphous silicon (i-a-Si: H) layer embedded in the hetero-junction, is adopted to chemically passivate the hetero-interface and can therefore significantly enhance the open circuit voltage V_{oc}.

The IBC-SHJ solar cells, can not only avoid the front optical loss but also take advantage of hetero-junctions, leading to the high efficiency due to the improvement of J_{sc} and V_{oc}.[5] These properties were sufficiently utilized by Panasonic and Kaneka and they achieved conversion efficiencies up to 25.6% and 26.6%, respectively,[6,7] which get close to the theoretical limit.[8]

The front surface field (FSF) structure, a stack of i-a-Si: H and P heavily doped a-Si (n^+-a-Si: H) layers, passivates the surface dangling bonds, and separates the photo-generated electron–hole pairs. As a consequence, the surface recombination can be effectively suppressed. The current density and voltage decrease dramatically since the surface passivation deteriorates.[9,10] In order to achieve the favorable chemical passivation, the i-a-Si: H layer is required to be deposited between c-Si and a-Si: H.[11–13] However, because of the higher absorption coefficient of a-Si: H than that of Si, a-Si: H will significantly reduce the spectrum response, therefore leading to the decrease of J_{sc} directly.[14,15] Besides, it is reported that each thickness increase by 10 nm can lead to the J_{sc} decrease by 1.5 mA/cm^2.[15] More importantly, the induced widen band gap n^+-a-Si: H, as a field passivated layer, is requisite to mitigate the loss of spectrum. Many researches about the front surface light enhance and surface passivation have been carried out.[16–20] The existing researches have been mainly focused on the i-a-Si: H deposition technology and its effects on the interface passivation of IBC-SHJ solar cells,[21] without fully considering the influence of the n^+-a-Si: H layer. To overcome this deficiency, the present study attempts to investigate the mechanism by integrating the optical loss and passivation of solar cells. Consequently, in this study, the n^+-a-Si:

*Project supported by the National Key Research Program of China (Grant Nos. 2018YFB1500500 and 2018YFB1500200), the National Natural Science Foundation of China (Grant Nos. 51602340, 51702355, and 61674167), and JKW Project, China (Grant No. 31512060106).

†Corresponding author. E-mail: taoke@ime.ac.cn
‡Corresponding author. E-mail: imesolar@126.com
§Corresponding author. E-mail: aiminl@dult.edu.com

© 2019 Chinese Physical Society and IOP Publishing Ltd

H properties of wider band gap on optical absorption, the effect of the doping concentration on the field passivation, and its combined action with chemical passivation are scrutinized by a two-dimensional simulation tool Sentaurus TCAD. All the parameters used in the modeling are consistent with those in experiments and measurements.

2. Device models and parameters extraction

2.1. Experiment

In this work, the solar-grade n-type c-Si wafers with (100) orientation are used in the experiment. The resistivity is 1–3 Ω·cm, and the thickness is 180 μm. All wafers are first cleaned by standard RCA, then dipped in HF to remove the native oxide layer formed at the surface of the wafers. Both intrinsic and doped a-Si: H thin films are deposited by multi-chamber plasma-enhanced chemical vapor deposition (PECVD). And the i-a-Si: H layers with the thicknesses of 3 nm, 5 nm, and 10 nm are prepared to study the surface chemical passivation performance.

The n^+-a-Si: H(O/C) thin films are deposited on quartz substrates using a gas mixture comprising silane (SiH_4), hydrogen (H_2), phosphorane (PH_3), and methane (CH_4) or nitrogen dioxide (NO_2) under the pressure of 70 Pa. The plasma power is 10 W, and the substrate temperature is 250 °C.

The effective minority carrier lifetime ($\tau_{\rm eff}$) measurements are performed on the samples with i-a-Si:H layers on the front and the back sides of the silicon wafers, respectively, which are realized by using the quasi-steady-state photoconductance (QSSPC) method (WCT-120, Sinton Instruments, USA). The optical properties are tested by a UV-3600 Plus UV–VIS–NIR spectrophotometer. The doping profiles of the doped a-Si thin films are measured by electrochemical capacitance–voltage (ECV) profiling (CVP21, WEP, Germany).

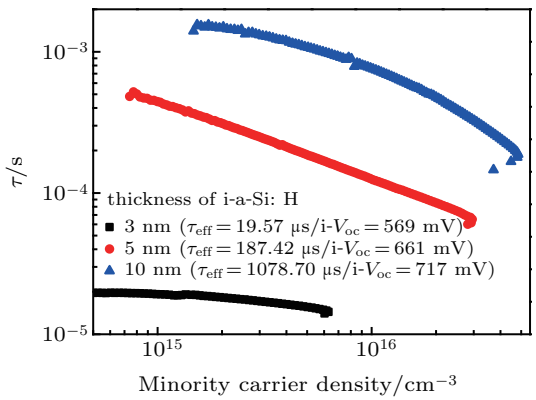


Fig. 1. Minority carrier lifetimes of samples with different i-a-Si: H layer thicknesses.

As shown in Fig. 1, the effective minority carrier lifetime $\tau_{\rm eff}$ decays dramatically with the thickness reduction. And so does the implied $V_{\rm oc}$ (i-$V_{\rm oc}$). At the low-injection level, $\tau_{\rm eff}$ can be expressed as

$$\frac{1}{\tau_{\rm eff}} = \frac{1}{\tau_{\rm bulk}} + \frac{2S}{W}. \tag{1}$$

The surface recombination velocity (S, cm/s) is used to represent the chemical passivation. The bulk lifetime $\tau_{\rm bulk}$ is impacted by the Auger recombination and Shockley–Read–Hall (SRH) recombination. W is the thickness of the sample. The $\tau_{\rm bulk}$ is simplified to be infinite, and S is calculated to be 10 cm/s, 100 cm/s, and 500 cm/s for the thicknesses of 10 nm, 5 nm, and 3 nm.

In IBC-SHJ, $J_{\rm sc}$ and $V_{\rm oc}$ increase dramatically when the front surface chemical passivation ameliorates,[9] which means that the thicker i-a-Si: H is beneficial for the chemical passivation. But thicker i-a-Si: H layer would induce optical loss in the front surface. The 5 nm thick i-a-Si: H is chosen to provide chemical passivation in the simulation.

As shown in Fig. 2, the optical band gaps of five n^+-a-Si: H materials, including microcrystalline silicon (μc-Si), amorphous silicon (a-Si), amorphous silicon carbide (a-SiC), and amorphous silicon oxide (a-SiO_x), increase from 1.52 eV to 2.30 eV, which are calculated by Tauc's equation

$$[\alpha(\upsilon)h\upsilon]^{1/2} = B\left(h\upsilon - E_{\rm g}\right), \tag{2}$$

with

$$t = (1-r)^2 \exp(\alpha d), \tag{3}$$

where $\alpha(\upsilon)$ is the absorption coefficient, $h\upsilon$ is the incident photon energy, B is a proportional constant,[22] t is the transmittance. r is the reflectivity, and d is the thin film thickness.

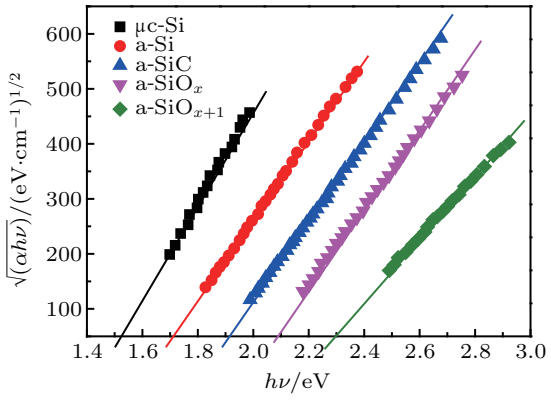


Fig. 2. Tauc's plots of optical absorption spectra of different n^+-a-Si: H materials.

The transmission and reflectance spectra of different P doped Si-based alloy materials are tested by the UV-3600 Plus UV–VIS–NIR spectrophotometer. The band gap width of different n^+-a-Si: H materials is in effect modulated by altering the a-Si morphology or impurity compound.

2.2. Device models

The simulator Sentaurus TCAD is extensively used for modeling solar cells based on the calculation of Possion equation and carrier continuity equation. The unit cell of the IBC-SHJ solar cells studied in this case is shown in Fig. 3. The substrate is an N type c-Si wafer with thickness of 180 μm. On the front textured surface, the FSF layer, a stack of 5 nm i-a-Si: H and 10 nm n^+-a-Si: H, is deposited. Then a 75 nm SiN_x layer is deposited as anti reflection (AR) coating. The P doped amorphous silicon (n^+-a-Si: H) and B doped amorphous silicon (p^+-a-Si: H) are prepared on the back side in an interdigital pattern. The lateral dimensions of the n-strips and p-strips are 450 μm and 150 μm, respectively. And the gap is set to be 10 μm. The other parameters are listed in Table 1 and the state density distributions of the three types of a-Si are based on Ref. [23]. In this work, the optical modeling is performed by means of ray tracing method combined with optical generation model and complex refractive index model. The drift–diffusion model, thermionic emission model, and trap-assist tunneling model are applied to describe carriers' transportation. The SRH recombination model, surface recombination model, and Auger recombination model are used to describe the recombination process in the cell. In addition, the energy band gap narrowing model, mobility model, and quantum potential model are also taken into consideration.

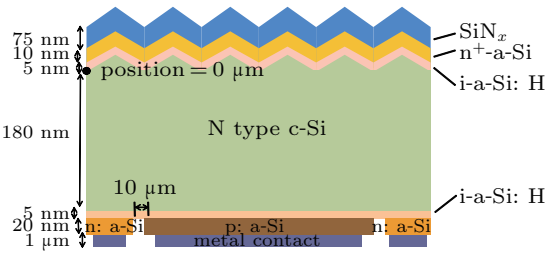


Fig. 3. Schematic structure of the simulated IBC-SHJ solar cells.

Table 1. Default parameters used in the simulation.

Material	E_g/eV	χ/eV	Doping concentration/cm^{-3}
Si	1.12	4.1	2×10^{15}
i-a-Si: H	1.70	3.8	2×10^{15}
p^+-a-Si: H (back)	1.65	3.8	ECV data
n^+-a-Si: H (back)	1.72	3.7	ECV data
n^+-a-Si: H (front)	1.52–2.30	3.7	1×10^{17}–1×10^{20}

The substrate doping is set to be 2×10^{15} cm^{-3} to match the wafer's resistivity. The effective doping concentrations of n^+-a-Si: H and p^+-a-Si: H are imported according to the ECV measurement results, as shown in Fig. 4. The doping concentration of the n^+ Si-based alloy materials is set from 1×10^{17} cm^{-3} to 1×10^{20} cm^{-3}, under the assumption of complete ionization.

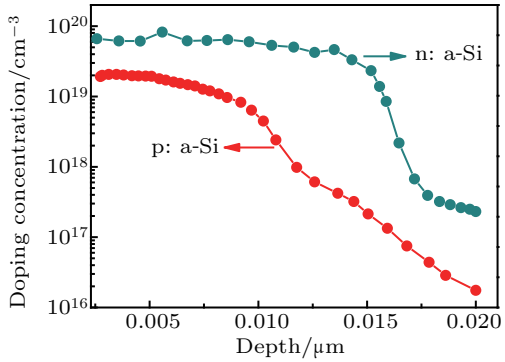


Fig. 4. Doping concentrations of n^+-a-Si: H and p^+-a-Si: H thin films on the back of IBC-SHJ solar cells.

The energy band model is based on the following equation:[24]

$$E_g(T) = E_g(0) - \frac{\alpha T^2}{T+\beta}, \tag{4}$$

where $E_g(0)$ is the band gap energy at 0 K, T is the thermal temperature, and α and β are the material parameters. The electron affinity χ is the difference between the lowest energy in the conduction band and the vacuum level, as described by

$$\chi(T) = \chi_0 + \frac{(\alpha+\alpha_2)T^2}{2(T+\beta+\beta_2)} + C_{\text{Bgn2Chi}}\cdot E_{\text{bgn}}, \tag{5}$$

where χ_0 and C_{Bgn2Chi} are adjustable parameters, and the default of C_{Bgn2Chi} is 0.5 in Sentaurus. In this simulation, the electron affinity is assumed to be constant for various band gaps.[22] Five kinds of n^+ Si-based alloy materials with band gaps of 1.52 eV, 1.72 eV, 1.92 eV, 2.10 eV, and 2.30 eV are simulated. The band gaps are determined from Fig. 2.

3. Results and discussion

3.1. Influence of band gap on optical properties

The energy band diagram of n^+-a-Si: H/i-a-Si: H/c-Si/i-a-Si: H/p^+-a-Si: H in thermal equilibrium is shown in Fig. 5. The doping concentration of n^+-a-Si: H is 6×10^{19} cm^{-3}. It is shown that the application of n^+-a-Si: H with different band gaps on the front surface will neither cause the bend of the energy band, nor the change of the field passivation.

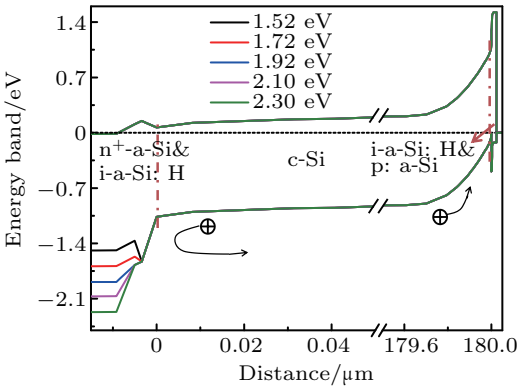


Fig. 5. Energy band diagram of n^+-a-Si: H/i-a-Si: H/c-Si/i-a-Si: H/p^+-a-Si: H with different band gaps in thermal equilibrium.

The reason is that the constant doping concentration of n^+-a-Si: H defines the position of the Fermi level. And the bending does not vary with the constant Fermi level position. Thus, the bending at the i-a-Si: H/c-Si interface is not influenced by the band gap of n^+-a-Si: H. Although the interface band bending does not change, the band structure on the front surface is still different. Figure 6 shows the integral photo-generated carrier in the entire substrate section of five n^+-a-Si: H materials under AM1.5 illumination. The number of photo-generated carriers increases with the enhancement of the band gap, which results from the fact that with the band gap widening, the photons in the short-wavelength range are not absorbed by the passivation stack, and thus can be effectively utilized by the substrate.

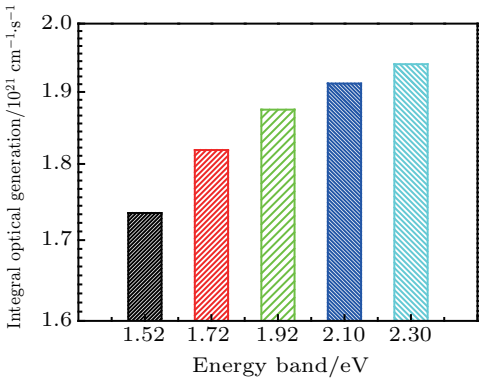


Fig. 6. Integral photo-generated carriers in the entire substrate section with different band gaps under AM1.5 illumination.

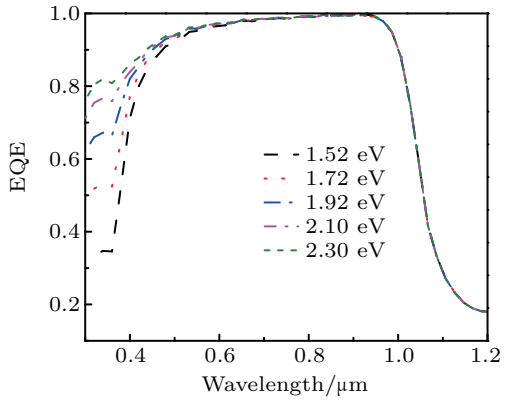


Fig. 7. EQE data of IBC-SHJ with n^+-a-Si: H thin films of different band gaps.

It can be seen from the external quantum efficiency (EQE) curve of the IBC-SHJ solar cells in Fig. 7 that due to the reduction of the absorption loss of photons by the passivation stack, the EQE is improved under the same field passivation. Compared with the case of band gap 1.52 eV, the weighted average EQE of 2.30 eV is increased by 12% according to the equation

$$\mathrm{EQE} = \frac{N_{\mathrm{ph}}}{N_{\mathrm{in}}}, \tag{6}$$

where N_{ph} is the photon-generated carriers collected in the terminal, and N_{in} is the total input photons. Therefore, increasing the bandgap width of the n^+-a-Si: H material can effectively improve the output photon current density.

3.2. Influence of doping concentration on field passivation

The energy band diagram of n^+-a-Si: H/i-a-Si: H/c-Si/i-a-Si: H/ p^+-a-Si: H with different doping concentration under thermal equilibrium is shown in Fig. 8. The band gap of n^+-a-Si: H is set to be 2.30 eV. As is seen, the band bending at the i-a-Si:H/c-Si interface changes with the doping concentration. With the increasing doping concentration, the energy band bends downward more seriously, which creates a higher barrier for holes. That is to say, the field passivation becomes stronger, and more holes can be driven back to the substrate.

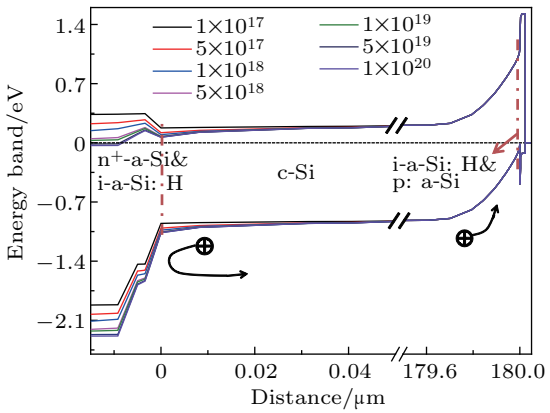


Fig. 8. Energy band diagram of n^+-a-Si: H/i-a-Si: H/c-Si/i-a-Si: H/p^+-a-Si: H with different doping concentration (in cm^{-3}) in thermal equilibrium.

The band bending at the interface can also be attributed to the change of the Fermi level. The higher the doping concentration is, the closer the Fermi level is to the conduction band, as shown by the following equation:

$$E_{\mathrm{F}} = E_{\mathrm{c}} + k_0 T \left(\frac{N_{\mathrm{D}}}{N_{\mathrm{c}}} \right), \tag{7}$$

where E_{F} is the Fermi level, E_{c} is the conduction band, k is the Boltzmann constant, N_{D} is the donor concentration, and N_{c} is the effective state density of the conduction band. In general, since $N_{\mathrm{c}} > N_{\mathrm{D}}$, the second term is negative.

The separation of electron–hole pairs on the front surface is due to the selection of the electric field. As shown in Fig. 9, the electric field becomes stronger because of the higher doping concentration of n^+-a-Si: H, and thus generates a stronger driving force to the holes. The change of the electric field corresponds to the energy band diagram in Fig. 10. Since the electric field results from the energy band bending, the more serious the energy band bends, the stronger the field becomes.

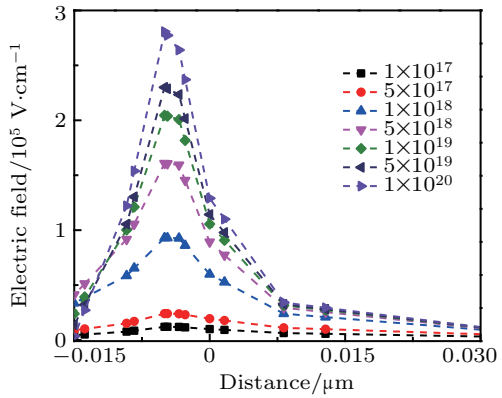


Fig. 9. Electric field on the front surface of different doping concentrations (in cm^{-3}).

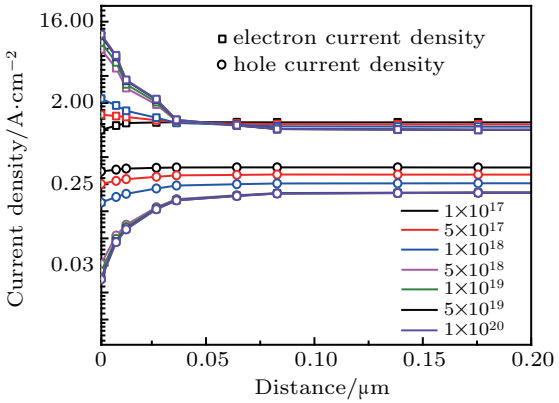


Fig. 10. Electron and hole current densities near IBC-SHJ front surface with different doping concentrations (in cm^{-3}).

Figure 10 shows the electron and the hole current densities near the front surface under the condition of different doping concentrations when the band gap is 2.30 eV. The electron current density increases rapidly with the increase of the doping concentration, which is contrary to the situation of the hole current density. The field effect strongly reduces the density of one type of carriers at the interface. The higher doping concentration results in the higher electric field, which can attract more majority carriers to the front surface. While it drives the minority carriers away from the front surface. Thus, the recombination of the carriers is reduced, which contributes to a higher carrier lifetime.

3.3. Chemical passivation and field passivation

The mutual action between chemical and field passivations on the front surface is also considered. As shown in Fig. 11, the electric field intensity is extracted at 0 μm in Fig. 9, the short circuit current J_{sc}, open circuit voltage V_{oc}, filling factor FF, and efficiency E_{ff} under different electric field passivation and chemical passivation are present. The surface recombination velocity, S varies from 10 cm/s to 500 cm/s to represent the chemical passivation quality from excellent to poor when ignoring the i-a-Si: H thickness.

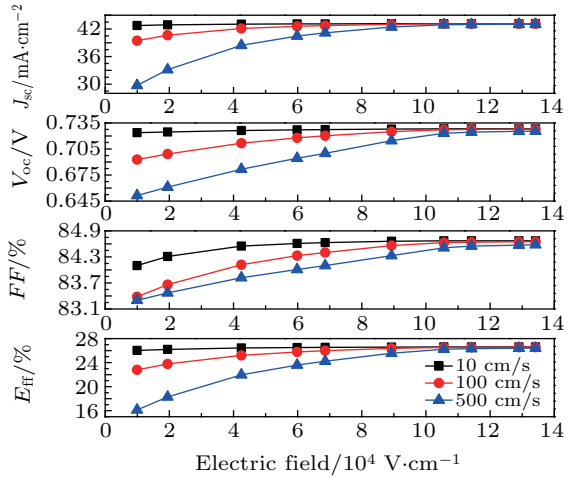


Fig. 11. The J_{sc}, V_{oc}, FF, and E_{ff} due to the total effect of chemical passivation and electric field passivation.

It can be seen that with the same chemical passivation, the J_{sc}, V_{oc}, FF, and E_{ff} increase with the increasing electric field on the front surface. E_{ff} decreases from 26.57% to 22.81% when the electric field reduces from 1.3×10^5 V/cm to 1×10^4 V/cm when S is 100 cm/s. And E_{ff} decreases from 26.41% to 16.13% when the electric field reduces from 1.3×10^5 V/cm to 1×10^4 V/cm with S of 500 cm/s. Under the condition of the same electric field passivation, the J_{sc}, V_{oc}, FF, and E_{ff} decay with the worsening chemical passivation. When the electric field passivation is strong ($> 1.0 \times 10^5$ V/cm), the chemical passivation has no significant effect on the J_{sc}, V_{oc}, FF, and E_{ff}. When the electric field strength is 1.3×10^5 V/cm, E_{ff} decreases from 26.57% to 26.41% with S increasing from 10 cm/s to 500 cm/s, resulting in only 0.16% reduction with inferior chemical passivation. Thus, the role of the field passivation cannot be ignored, especially in the case of thin intrinsic passivation layers and poor chemical passivation.

The S of 100 cm/s represents the poor chemical passivation condition (5 nm i-a-Si: H layer). The optical and electrical properties of n$^+$-a-Si thin films are compared comprehensively. Figure 12 shows the changes of the J_{sc}, V_{oc}, FF, and E_{ff} with different doping concentrations and band gaps.

It is manifested that J_{sc} enhances with the increasing band gap width and doping concentration. The broadening of the band gap can reduce the light absorption by amorphous silicon and increase the absorption in the substrate. The high doping concentration can enhance the field passivation of the cell, and thus significantly improve the V_{oc}. The FF increases with the increase of the doping concentration as the recombination is suppressed. The combined effect of these two factors enables the IBC-SHJ to achieve a conversion efficiency of over 26% in spite of the poor chemical passivation.

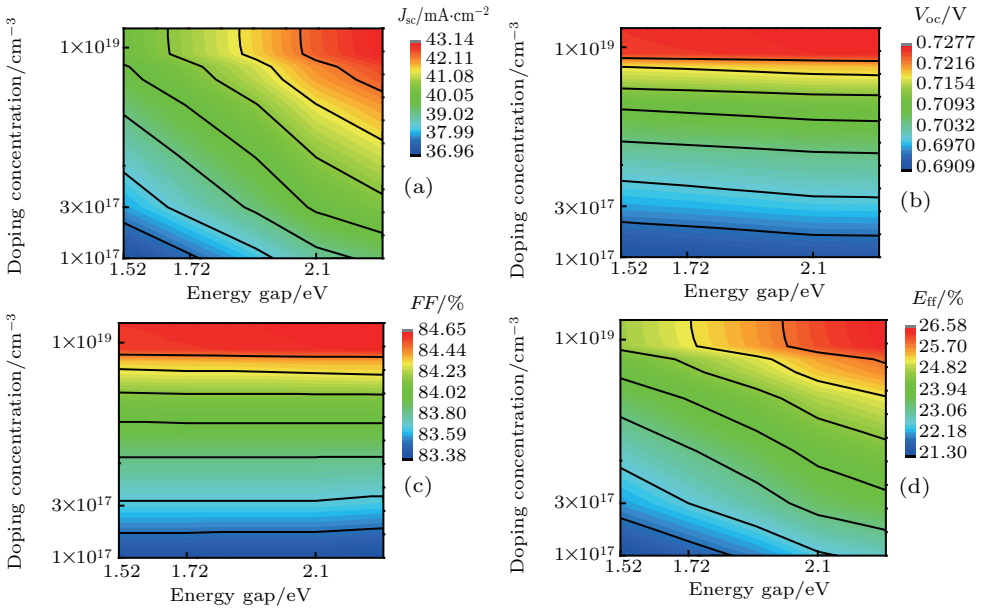


Fig. 12. The (a) J_{sc}, (b) V_{oc}, (c) FF, and (d) E_{ff} of IBC-SHJ solar cells with different doping concentrations and band gaps.

4. Conclusion

In the present study, the n$^+$-a-Si: H materials with different band gaps and doping concentrations are applied to the FSF of IBC-SHJ solar cells, and investigated by Sentaurus TCAD tools. The results show that the light absorption of the stack of amorphous silicon films decreases with the widening band gap, which generates more photo-generated carriers and improves the external quantum efficiency of the solar cells. However, the wide band gaps do not contribute to the band bending at the i-a-Si: H/c-Si interface, and thus have no effect on the front field passivation. And the bending is mainly affected by the doping concentration. With the increasing doping concentration, the energy band is more seriously bending, which means a higher potential barrier for holes.

According to the distribution of the electric field and carrier current density on the front surface, it is shown that the electric field becomes stronger, and enhances the selectivity of electrons while restrains the transportation of minority carriers, and the recombination of two carriers is reduced. In addition, the relationship between the field passivation and the chemical passivation is also investigated. When the chemical passivation is constant, J_{sc}, V_{oc}, FF, and E_{ff} of IBC-SHJ increase with the enhancement of the field passivation. When the field passivation is strong enough ($> 1.0 \times 10^5$ V/cm), the decrease of E_{ff} due to the deterioration in chemical passivation is only 0.21%. The J_{sc} increases obviously with the increasing band gap width, and V_{oc} increases obviously with the increasing doping concentration. In the case of poor chemical passivation (i-a-Si: H: 5 nm), the efficiency of IBC-SHJ solar cells still achieves over 26% by applying wide band gap and heavily doped n$^+$-a-Si: H materials.

References

[1] Schwartz R J and Lammert M D 1975 *IEEE Electron Devices Meeting 1975 International*

[2] Smith D D and Reich G 2016 *Photovoltaic Specialists Conference (PVSC) IEEE 43rd*

[3] Adachi D, Hernandez J L and Yamamoto K 2015 *Appl. Phys. Lett.* **107** 233506

[4] Taguchi M, Yano A, Tohoda S, Matsuyama K, Nishikaw T, Fujita K and Maruyama E 2014 *IEEE J. Photovoltaics* **4** 96

[5] Lu M, Bowden S, Das U and Birkmire R 2007 *Appl. Phys. Lett.* **91** 063507

[6] Masuko K, Shigematsu M, Hashiguchi T and Fujishima D 2014 *IEEE J. Photovoltaics* **4** 1433

[7] Yoshikawa K, Kawasaki H, Yoshida W and Irie T 2017 *Nat. Energy* **2** 17032

[8] Richter A, Hermle M and Glunz S W 2013 *IEEE J. Photovoltaics* **3** 1184

[9] Lu M, Das U, Bowden S, Hegedus S and Birkmire R 2009 *Proceedings of 34th IEEE PVSC USA*

[10] Dioufa D, Kleider J P, Desrues T and Ribeyron P J 2009 *Mater. Sci. Eng. B* **159-160** 291

[11] Xiao Y P, Wei X Q and Zhou L 2017 *Chin. Phys. B* **26** 048104

[12] Das U K, Burrows M Z, Lu M, Bowden S and Birkmire R 2008 *Appl. Phys. Lett.* **92** 063504

[13] Lu M, Das U, Bowden S, Hegedus S and Birkmire R 2011 *Prog. Photovolt: Res. Appl.* **19** 326

[14] Yu J, Zhou J, Bian J, Shi J, Meng F and Liu Z 2018 *IEEE 7th World Conference on Photovoltaic Energy Conversion* (WCPEC)

[15] Holman Z C, Descoeudres A, Barraud L, Fernandez F Z, Seif J P, Wolf S D and Ballif C 2012 *IEEE J. Photovoltaic* **2** 7

[16] Qiu H B, Li H Q, Liu B W, Zhang X and Shen Z N 2014 *Chin. Phys. B* **23** 027301

[17] Xiao H Q, Zhou C L, Cao X N, Wang W J, Zhao L, Li H L and Diao H W 2009 *Chin. Phys. Lett.* **26** 088102

[18] Zhang Y, Cao Y and Yang M 2017 *Chin. Phys. Lett.* **34** 038101

[19] Zhang J N, Wang L, Dai Z, Tang X, Liu Y B and Yang D R 2017 *Chin. Phys. Lett.* **34** 028801

[20] Zhan F, Wang H L, He J F, Wang J, Huang S S, Ni H Q and Niu Z C 2011 *Chin. Phys. Lett.* **28** 047802

[21] Salomon B P, Tomasib A, Lachenalc D and Badela N 2018 *Sol. Energy* **175** 60

[22] Rath J K 2003 *Sol. Energy Mater. Sol. Cells* **76** 431

[23] Munos D 2011 *7th Workshop on the Future Direction of Photovoltaics (by JSPS 175th committee)*

[24] Bludau W, Onton A and Heinke W 1974 *J. Appl. Phys.* **45** 1846